DISEASES AND DISORDERS

Prevention and treatment of autoimmune diseases with plant virus nanoparticles

Roberta Zampieri[1,2]*, Annalisa Brozzetti[3]*, Eva Pericolini[4]*, Elena Bartoloni[3], Elena Gabrielli[3], Elena Roselletti[3], George Lomonosoff[5], Yulia Meshcheriakova[5], Luca Santi[6], Francesca Imperatori[6], Matilde Merlin[1], Elisa Tinazzi[7], Francesco Dotta[8], Laura Nigi[8,9], Guido Sebastiani[8,9], Mario Pezzotti[1], Alberto Falorni[3], Linda Avesani[1†]

Plant viruses are natural, self-assembling nanostructures with versatile and genetically programmable shells, making them useful in diverse applications ranging from the development of new materials to diagnostics and therapeutics. Here, we describe the design and synthesis of plant virus nanoparticles displaying peptides associated with two different autoimmune diseases. Using animal models, we show that the recombinant nanoparticles can prevent autoimmune diabetes and ameliorate rheumatoid arthritis. In both cases, this effect is based on a strictly peptide-related mechanism in which the virus nanoparticle acts both as a peptide scaffold and as an adjuvant, showing an overlapping mechanism of action. This successful preclinical testing could pave the way for the development of plant viruses for the clinical treatment of human autoimmune diseases.

INTRODUCTION

Viruses are proteinaceous nanoscale structures that have evolved to deliver their cargo of nucleic acids efficiently into cells, enabling replication and the production of new viruses. This confers a number of attractive properties that can be exploited in the fields of materials science, electronics, agriculture, and medicine (1). The self-assembly of virus capsids from one or more types of coat protein subunit forms virus nanoparticles (VNPs) that are homogeneous in size and shape. The genetically encoded coat proteins can be modified to incorporate new sequences and can be synthesized using rapid and scalable manufacturing platforms. Additional functionalities can also be introduced by chemical conjugation (1).

VNPs can be based on mammalian viruses or bacteriophages, but plant VNPs (pVNPs) share all the beneficial characteristics listed above with the further advantage that they are unable to replicate in mammals, making them safer for medical applications (2). The scalable production of pVNPs can be achieved by molecular farming in natural plant hosts (3). Thus far, pVNPs have been used for bioimaging applications, cancer therapy, and the development of vaccines presenting antigens and peptides derived from pathogens (3, 4). Another promising medical application of pVNPs is the development of therapeutic vaccines displaying immunodominant peptides associated with autoimmune diseases, which can be used to induce immunotolerance. We investigated the potential of this approach by focusing on two common human autoimmune diseases: type 1 diabetes mellitus (T1D) and rheumatoid arthritis (RA).

T1D is an organ-specific disease characterized by the destruction of pancreatic islet β-cells mediated by cellular and humoral immune responses (5). These responses target several autoantigens including the 65-kDa isoform of glutamic acid decarboxylase (GAD65), which has been identified as one of the major T1D autoantigens both in humans and in nonobese diabetic (NOD) mice (6). The NOD mouse strain is one of the best animal models of human autoimmune diabetes and spontaneously develops many of the disease features seen in human T1D (7). Preclinical studies in NOD mice have shown that protein or peptide vaccines based on GAD65 can prevent diabetes (8). However, the role of GAD65 peptides spanning residues 524 to 543 of the native protein (p524) remains controversial, with several reports suggesting a protective role either individually or combined with other peptides (9–12). Notably, a challenge with p524 triggered the expansion of CD4$^+$ CD25$^+$ Foxp3$^+$ suppressive T cells in vitro, and those cells were later able to inhibit diabetes in a cotransfer model (10). In silico modeling suggests that the negatively charged surface of p524 may help it to bind two major histocompatibility complex class II antigen chains and may thus improve its stability (10).

RA is a systemic disease involving the loss of tolerance to various citrullinated antigens (13). This results in the activation of autoreactive T cells and the production of inflammatory cytokines that lead to progressive synovial inflammation. Most patients with RA (50 to 80%) are seropositive for two types of autoantibody: rheumatoid factor [which recognizes the Fc portion of immunoglobulin G (IgG)] and anti-citrullinated protein antibody (ACPA), which recognizes citrullinated proteins and peptides (14). Seropositive RA patients tend to experience a more severe disease course than seronegative patients, with a higher risk of joint erosion and a lower probability of disease-free remission in response to conventional therapies (14). However, seronegative patients may have a more active form of the disease, with similar radiographic damage at presentation and a slower treatment response compared to seropositive patients, suggesting that seronegative RA may have a worse outcome than previously understood (15). We recently demonstrated that pLip1 and pFADK2 are immunodominant peptides associated with patients seronegative for rheumatoid factor and ACPA, suggesting that immunization with these peptides may allow the treatment of seronegative RA (16).

[1]Department of Biotechnology, University of Verona, Verona, Italy. [2]Diamante srl, Strada Le Grazie, 15, 37134 Verona, Italy. [3]Department of Medicine, University of Perugia, Perugia, Italy. [4]Department of Surgical, Medical, Dental and Morphological Sciences with interest in Transplant, Oncological and Regenerative Medicine, University of Modena and Reggio Emilia, Modena, Italy. [5]Department of Biological Chemistry, John Innes Centre, Norwich, UK. [6]Department of Agriculture and Forest Sciences, University of La Tuscia, Viterbo, Italy. [7]Department of Medicine, University of Verona, Verona, Italy. [8]Diabetes Unit, Department of Medicine, Surgery and Neuroscience, University of Siena, Siena, Italy. [9]Umberto Di Mario Foundation ONLUS, Toscana Life Sciences, Siena, Italy.
*These authors contributed equally to this work.
†Corresponding author. Email: linda.avesani@univr.it

To investigate the suitability of pVNPs as a means to address T1D and RA, we designed pVNPs based on two different plant viruses: cowpea mosaic virus (CPMV) and tomato bushy stunt virus (TBSV) (*17*, *18*). CPMV has an icosahedral capsid, 30 nm in diameter, comprising 60 copies each of the large and small coat protein subunits. For the CPMV system, we used genome-free virus-like particles (VLPs) that have the same structural characteristics as the parent virus. In contrast, TBSV was produced as an infectious virus. TBSV also has an icosahedral, 30-nm capsid but is composed of 180 subunits of a single capsid protein. We used genetic engineering to express immunodominant peptides associated with T1D (p524) on CPMV and RA (pLip1 and pFADK2) on TBSV. We then tested the ability of the pVNPs to prevent T1D or reduce the severity of RA in appropriate animal disease models: NOD mice for T1D, and dilute, brown, and non-agouti (DBA) mice for RA, based on their susceptibility to collagen-induced arthritis (CIA) (*19*).

RESULTS

Production of self-assembling VNPs in plants

CPMV-based VLPs were produced in the leaves of *Nicotiana benthamiana* plants by agroinfiltration. The sequence of the CPMV small coat protein subunit (VP60) was engineered to display the GAD65 peptide p524 on the outer surface of the assembled particle. The wild-type p524 sequence (SRLSKVAPVIKARMM) has a suboptimal isoelectric point (pI) for display (*17*), so the sequence was adjusted (p524opt: DSRLSKVAPVIKARMMED) to achieve a pI of 8.59. The p524opt sequence was inserted within the βB-βC loop of the small coat protein subunit in pEAQ-HT-VP60 to produce vector pEAQ-HT-VP60.p524opt. *N. benthamiana* leaves were infiltrated with *Agrobacterium tumefaciens* carrying pEAQ-HT-VP60.p524opt (or pEAQ-HT-VP60 as a control) together with another *A. tumefaciens* strain carrying pEAQ-HT-24K, encoding the large coat protein subunit.

Extracts of leaves infiltrated with pEAQ-HT-24K plus either pEAQ-HT-VP60.p524opt or pEAQ-HT-VP60 were prepared 6 days post-infiltration (dpi) for analysis by Western blot using an anti-CPMV antiserum (Fig. 1A). This revealed the presence of the processed large and small coat proteins in both samples, with the small coat protein derived from pEAQ-HT-VP60.p524opt migrating more slowly than that from pEAQ-HT-VP60, consistent with the presence of the p524opt peptide. The virus particles were isolated from *N. benthamiana* leaf tissue, resulting in yields of 100 mg of purified CPMV per kilogram of leaf fresh weight (LFW) and 10 mg of purified CPMV.p524opt per kilogram of LFW as determined by
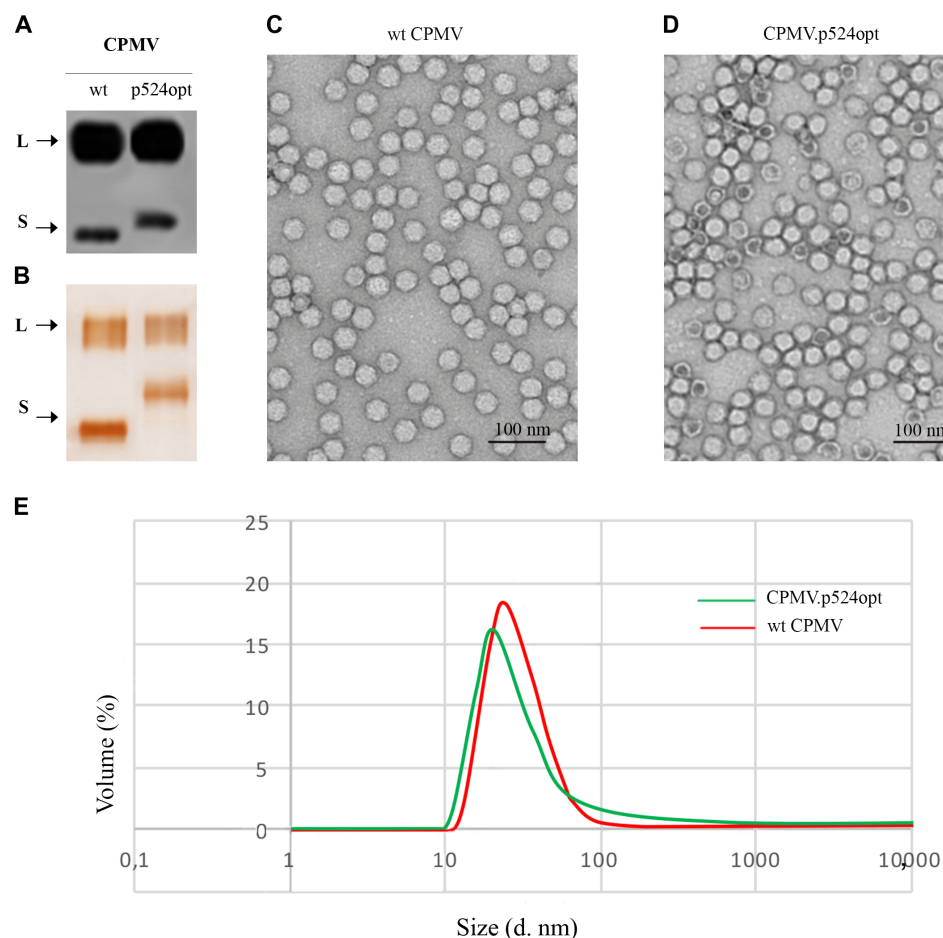

Fig. 1. Characterization of pVNPs derived from CPMV. Wild-type particles (wt CPMV) and particles displaying the p524opt peptide (CPMV.p524opt) were characterized and compared after purification from *N. benthamiana* leaves. Gel electrophoresis under denaturing conditions was followed by (**A**) silver staining and (**B**) Western blot analysis to assess the purity of the particles. The small subunit (S) and large subunit (L) were detected in both cases. The structural conformation of the purified particles was confirmed by TEM (**C** and **D**) and DLS analysis (**E**).

a silver staining (Fig. 1B), which also indicated that the p524opt peptide was displayed on the surface of the particles. Transmission electron microscopy (TEM) showed no structural differences between CPMV and CPMV.p524opt, confirming that the peptide did not interfere with self-assembly (Fig. 1, C and D). Likewise, dynamic light scattering (DLS) analysis showed that CPMV and CPMV.p524opt had a similar hydrodynamic radius (Fig. 1E).

TBSV-based pVNPs were also produced in *N. benthamiana* plants, following the engineering of the surface-exposed C terminus of the coat protein to display pLIP1 (ASVLANVAQAFE) or pFADK2 (AKVLANLAHPPA). In vitro transcribed genomic RNA encoding the wild-type TBSV and modified TBSV.pLIP1 and TBSV.pFADK2 coat proteins was used for the infection of *N. benthamiana* plants. Infected plant material was collected when symptoms of virus disease appeared, and the pVNPs were purified and analyzed by Western blot and silver staining as above (Fig. 2A). We achieved yields of 65 mg/kg LFW for wild-type TBSV, 72 mg/kg for TBSV.pLIP1, and 114 mg/kg for TBSV.pFADK2. TEM (Fig. 2, B to D) and DLS (Fig. 2E) analysis revealed that the modified particles assembled in the same manner as the wild-type virus.

CPMV.p524opt achieves the partial prevention of autoimmune diabetes in mice

We treated NOD female mice before the onset of insulitis by intraperitoneal injection with synthetic peptides (p524 and p524opt), pVNPs (one or two doses of CPMV.p524opt), or wild-type CPMV as a control (Fig. 3 and fig. S1). Neither of the peptides altered the disease course, but the two doses of CPMV.p524opt nanoparticles induced a protective effect compared to the other treatments (overall $P = 0.01$, log-rank test). More specifically (Fig. 3A), Kaplan-Meier analysis showed a significantly lower progression to diabetes for NOD mice treated with two doses of CPMV.p524opt compared to wild-type CPMV ($P = 0.04$), p524opt ($P = 0.008$), or p524 ($P = 0.001$). The untreated group showed a survival curve identical to the wild-type CPMV group: first clinical symptoms at 71 days of age, 30% disease prevalence at 121 days, 50% at 142 days, and 80% at 168 days. Comprehensive statistical comparisons among treatments are provided in fig. S1.

Nondiabetic NOD female mice were examined for islet infiltration at different time points (5, 10, and 27 weeks after the treatment). Histological analysis of pancreas samples showed a significant overall
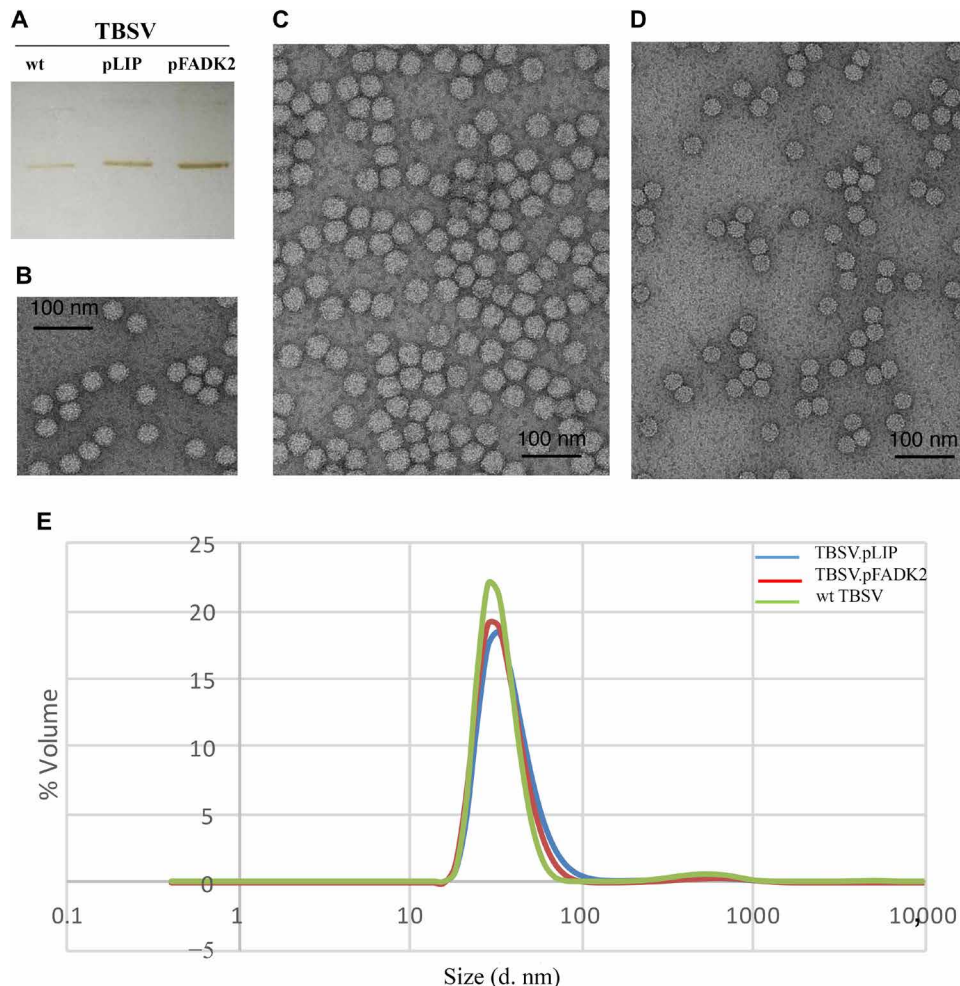
Fig. 2. Characterization of TBSV.pLip1 and TBSV.pFADK2. Wild-type particles (wt TBSV) and particles displaying the pLIP1 and pFADK2 peptides (TBSV.pLIP1 and TBSV.pFADK2, respectively) were analyzed after purification from infected *N. benthamiana* plants. Gel electrophoresis under denaturing conditions was followed by silver staining of the purified particles (**A**). The structural conformation of the purified wt TBSV (**B**), TBSV.pLIP1 (**C**), and TBSV.pFADK2 (**D**) particles was assessed by TEM and DLS analysis (**E**).
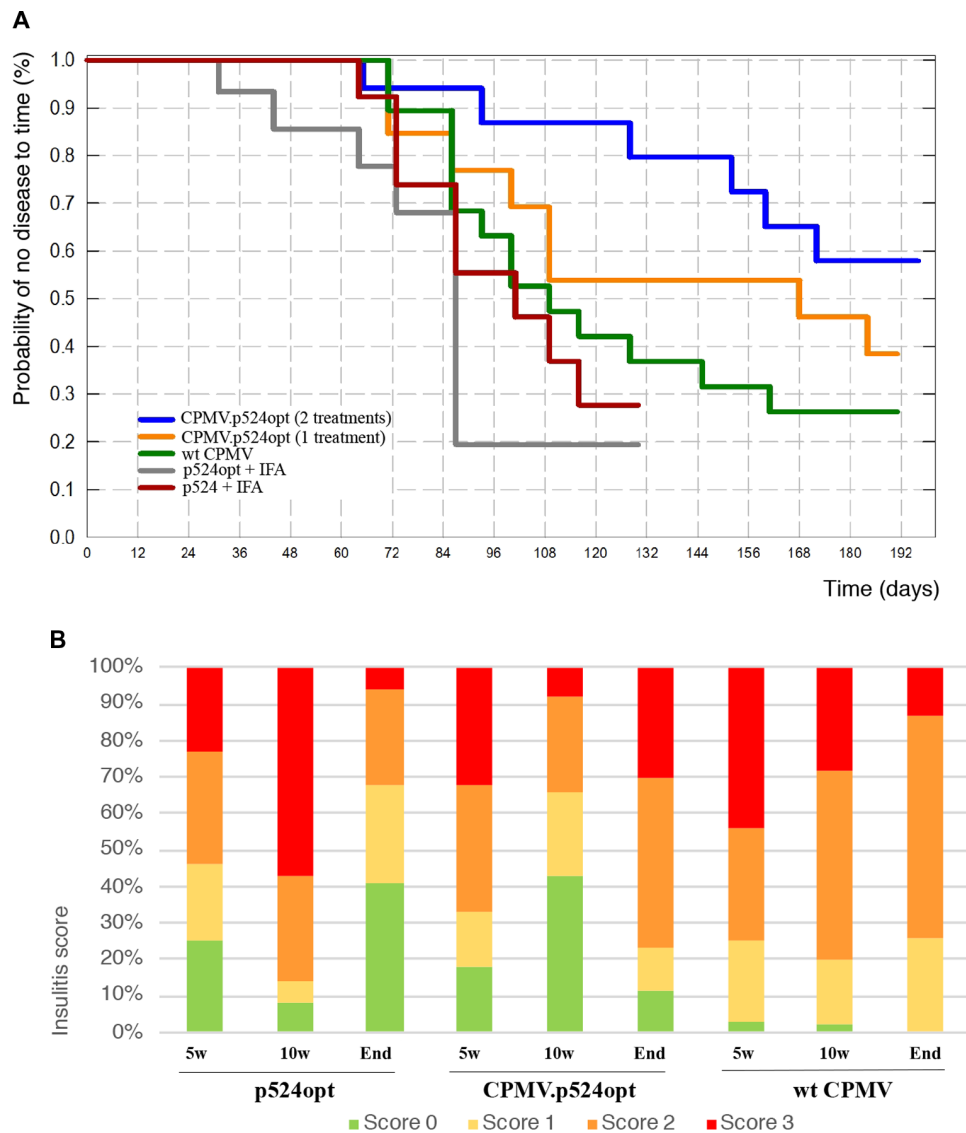
A

B

Fig. 3. Partial protection from autoimmune diabetes in NOD mice treated with CPMV-derived particles displaying the p524opt peptide. The survival curves of groups treated with CPMV-derived particles indicate partial protection from the onset of diabetes in mice treated twice with CPMV.p524opt (blue line) compared to all the other groups: wt CPMV (green line), p524opt synthetic peptide + IFA (red line), and p524 synthetic peptide + IFA (gray line). The single administration of CPMV.p524opt (yellow line) did not prevent the onset of diabetes. The x axis indicates the number of days after the first treatment (**A**). The histopathology of pancreatic islet cells was determined in subsets of the treated mice by counting infiltrated cells. After 5 and 10 weeks of treatment (5w and 10w) and at the end of the treatment, some animals were euthanized to characterize the progression of the disease; CPMV.p524opt is the animal group that received double treatment (**B**).

difference in insulitis score among the different treatment groups (Kruskal-Wallis test, $P < 0.0001$). More specifically (Fig. 3B), a significant difference was observed at all three time points between animals treated with CPMV.p524opt and those treated with the wild-type virus ($P < 0.0001$), as well as at 10 and 27 weeks between animals treated with CPMV.p524opt and those treated with p524 ($P < 0.0001$).

Foxp3[+] regulatory T (T_{reg}) cells play a key role in self-tolerance, so we investigated whether CPMV.p524opt increased the number of Foxp3^{+} cells in the treated mice. Immunofluorescence analysis of pancreatic sections revealed a significantly lower ($P = 0.034$) number of Foxp3^{+} cells within and around islets in mice treated with CPMV.p524opt compared to those treated with wild-type CPMV (Fig. 4A).

Serum from all treatment groups was analyzed to identify soluble mediators, and the distribution among groups was determined by two-way orthogonal partial least squares discriminant analysis (OPLS-DA), indicating four distinct groups matching the different treatments (Fig. 4B). The corresponding scatter plot (Fig. 4C) revealed two principal components. The first (P1; horizontal axis) explains 34.5% of the variability and separates CPMV.p542opt 2 treatments + wt CPMV from CPMV.p524opt single treatment + p524. This reflects the activation of soluble mediators with different profiles depending on the treatment: mainly KC (keratinocyte chemoattractant), IL1a (interleukin-1a), IL13, eotaxin, and IL9 for wt CPMV but mainly MCP1 (monocyte chemoattractant protein 1), MIP1B (macrophage inflammatory protein 1B)/1A, IL12, IL10, RANTES, IFNγ (interferon-γ), and IL2
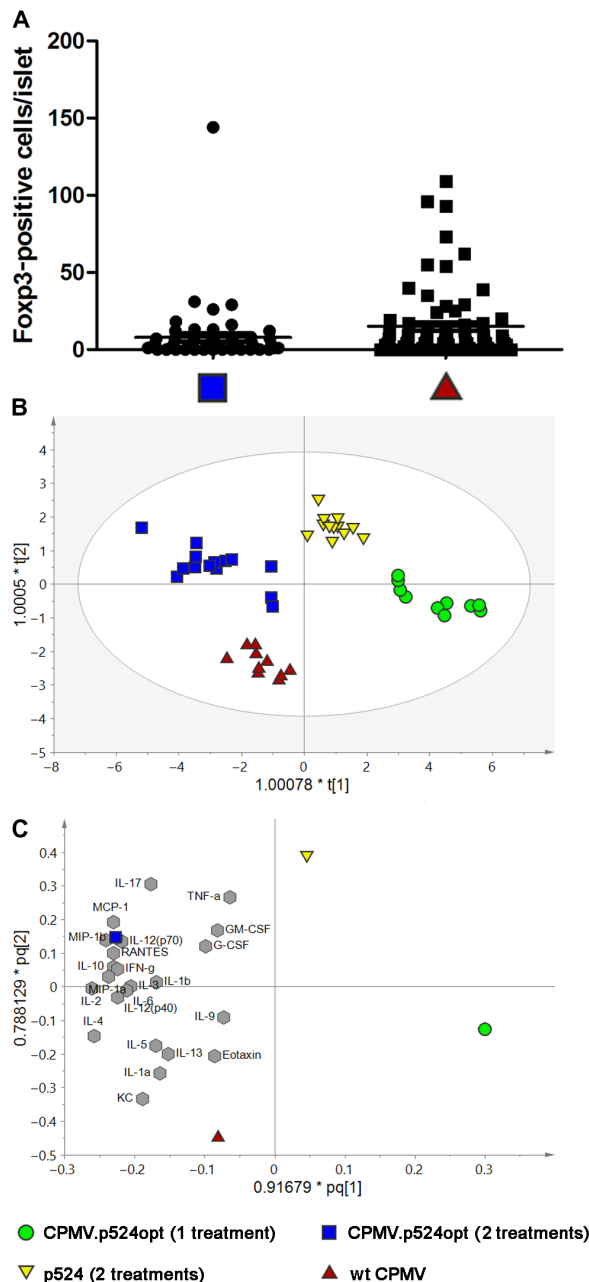
Fig. 4. T$_{reg}$ cell numbers and global cytokine profiles in NOD mice treated with CPMV-derived particles. Mice treated with two doses of CPMV.p524opt and mice treated with the wt CPMV particles show no significant difference in the number of Foxp3$^+$ T cells (**A**). OPLS-DA score scatter plot (**B**) and loading scatter plot (**C**) of the preclinical study model (explained variance = 44.7%) with two doses (blue square) or one dose (white circle) of CPMV.p524opt, with the wt CPMV (red triangle) and with p524 synthetic peptide (yellow triangle). OPLS-DA model = 3 + 6 + 0, R2X(cum) = 0.919, R2Y(cum) = 0.878, Q2(cum) = 0.764. In the loading scatter plot (C), the green dots show the contribution of each cytokine to the statistical classes listed above. The global cytokine profile shows the activation of different cytokines in mice treated twice with wt CPMV (red triangle) and CPMV.p524opt (blue square). Mice treated twice with the synthetic p524opt peptide (yellow triangle) or once with CPMV.p524opt (green circle) do not show specific activation profiles compared to the other treatment groups.

for CPMV.p524opt 2 treatments; the CPMV.p542opt 1 treatment shows the non-activation of the aforementioned cytokine profile rather than a specific signature. The second (P2; vertical axis) explains 10.2% of the variability and seems to correlate with the concentration of p524.

TBSV.pLIP1 and TBSV.pFADK2 reduce the severity of RA in mice

The first signs of arthritis in DBA mice appeared 28 days after collagen injection, and 100% of the immunized mice exhibited arthritis after 33 days. Figure 5 shows the effect of pVNPs and synthetic peptides administered starting 28 days after immunization compared to a negative control group treated with saline. The group treated with TBSV.pFADK2 (Fig. 5A) demonstrated a lower clinical score (days 31 to 60 after immunization) compared to mice treated with pFADK2 plus incomplete Freund's adjuvant (IFA), which is a remarkable improvement given the comparable disease symptoms on day 28. The effect on mice treated with TBSV.pFADK2 was similar to that of the positive control group injected with dexamethasone. However, at the end of the immunization period (day 28), TBSV.pFADK2 was administered only to those mice whose disease severity was higher than that of control group mice, thus supporting the greater efficacy of TBSV.pFADK2 (Fig. 5A).

Even better results were observed in the group treated with TBSV.pLIP1 (Fig. 5B). As above, the groups receiving the TBSV.pLIP1 and pLIP1 + IFA formulations had the same clinical arthritis score 28 days after immunization. However, the administration of TBSV.pLIP1 completely abolished all clinical signs of arthritis at the end of treatment, whereas mice treated with pLIP1 + IFA had similar arthritis scores on day 60 to mice treated with dexamethasone, although the former group was characterized by more severe arthritis at the beginning of treatment. Last, the comparison of TBSV.pFADK2, TBSV.pLIP1, and wild-type TBSV revealed that even wild-type TBSV induced partial protection (Fig. 5C), as also seen for the wild-type CPMV particles in the T1D model (Fig. 3A). Treatment with TBSV.pLIP1 was the most effective, eliminating all signs of arthritis by the end of the treatment period (Fig. 5B). The efficacy of TBSV.pFADK2 appeared similar to the wild-type TBSV, but it is important to consider that, by day 28, the group treated with TBSV.pFADK2 had a higher clinical score than the group treated with wild-type TBSV. These data support the hypothesis that intrinsic virus structures boost the regulatory activity of immunodominant peptides and work as an adjuvant.

Given the positive effect of the pLIP1 and pFADK2 peptides in mice when presented on the pVNPs, we tested the hypothesis that both peptides can induce the expansion of immunomodulatory cell populations. We therefore evaluated a panel of proinflammatory and anti-inflammatory cytokines in the serum, joints, and lymph nodes of the treated mice (Fig. 6C). We observed a general depletion of proinflammatory cytokines such as TNFα (tumor necrosis factor–α), IL17A IL1β, and IFNγ in the groups treated with TBSV and the synthetic peptides pLIP1 and pFADK2 + IFA, but treatment with TBSV.pLIP1 was associated with a more effective depletion of all proinflammatory cytokines in the lymph nodes and of TNFα and IL17A in serum, with no effect on cytokine levels in the joints. Furthermore, pFADK2 + IFA markedly reduced the levels of TNFα, IL17A, IL1β, and IFNγ in the lymph nodes and IL17A in the serum, as well as achieving a general trend toward the depletion of proinflammatory cytokines in the joints (significant in the case of IFNγ). On the other hand, treatment with TBSV.pFADK2 strongly reduced
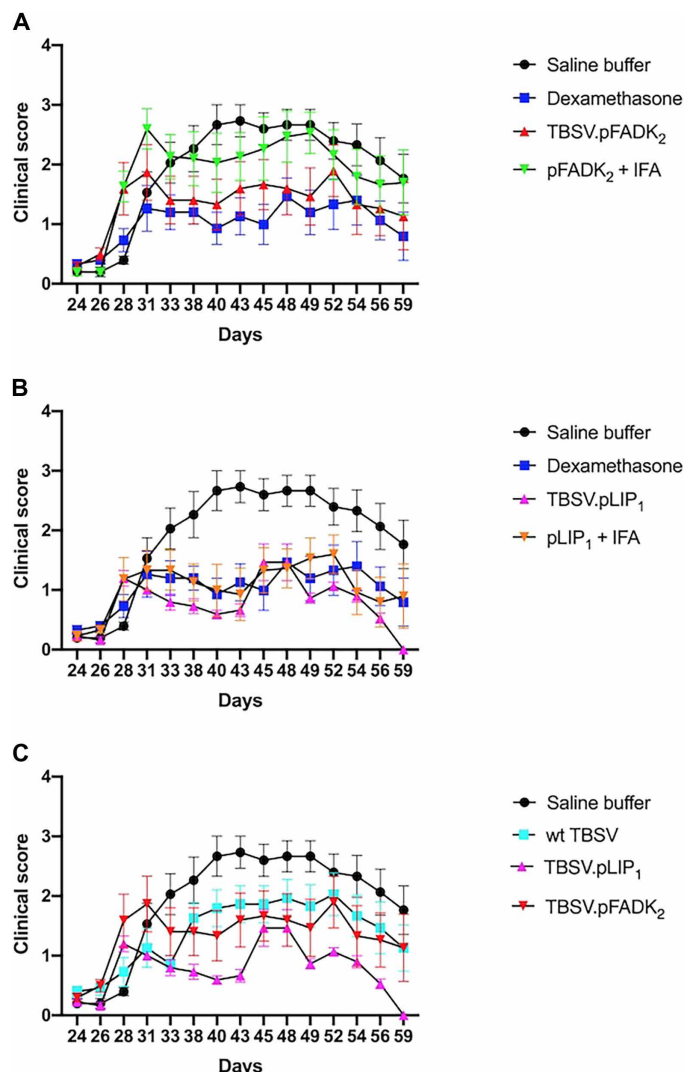
Fig. 5. Effect of TBSV-derived particles on the severity of CIA. Arthritic scores in each group were assessed every 2 to 3 days starting from days 24 to 59 after immunization. (**A**) Comparison of saline-treated CIA mice (control) to CIA mice treated with dexamethasone, TBSV.pFADK2, or pFADK2 + IFA. (**B**) Comparison of saline-treated CIA mice (control) to CIA mice treated with dexamethasone, TBSV.pLIP1, or pLIP1 + IFA. (**C**) Comparison of saline-treated CIA mice (control) to CIA mice treated with wt TBSV, TBSV.pLIP1, or TBSV.pFADK2. Each time point represents the mean arthritic score ± SEM (n = 5). Statistical significance was determined by applying the Kruskal-Wallis test followed by Dunn's multiple comparison test. Values of $P < 0.05$ were considered significant. Significance was established for CIA mice treated with dexamethasone versus saline-treated CIA mice and for CIA mice treated with TBSV.pLIP1 versus saline-treated CIA mice.

the levels of IL17A in lymph nodes and serum and IL1β and IFNγ in lymph nodes.

Treatment with dexamethasone resulted in the more effective modulation of all proinflammatory cytokines in lymph nodes, as well as TNFα, IL1β, and IFNγ in joints, and TNFα in serum. Moreover, the administration of dexamethasone and pFADK2 + IFA induced a therapeutic effect driven by TGFβ (transforming growth factor–β), a pleiotropic cytokine with potent regulatory and inflammatory activity. In contrast, TBSV.pLIP1 and TBSV.pFADK2 induced a more direct activation of IL10. Wild-type TBSV also partially induced the

production of TGFβ and IL10 in serum (Fig. 6B). The cytofluorimetric analysis of T_{reg} (CD25$^+$/Foxp3$^+$) cells in lymph nodes showed that TBSV.pFADK2 strongly increased the proportion of these cells, and a similar effect, although less pronounced, was observed for TBSV.pLIP1 and pLIP1 + IFA, whereas dexamethasone showed the most potent effect overall.

DISCUSSION

The development of VNPs for medical applications has thus far focused mainly on the delivery of drugs and imaging molecules to particular target cells (20–22). However, the ability of VNPs to display peptide antigens or epitopes has also resulted in their application as vaccines, for example, the display of pathogen-derived peptides as an active immunization strategy against infectious diseases or the display of self-antigens found on cancer cells as a means to turn the immune system against tumors (22). The investigation and preclinical testing of these approaches has generated a body of evidence that VNPs also have immunomodulatory effects: For example, pVNPs have been shown to suppress cancer cell proliferation and metastasis through the activation of both local (tumor microenvironment) and systemic anticancer immune responses involving the modulation of cytokine secretion and the activation states of different immune cell populations (21, 22). We therefore hypothesized that pVNPs displaying autoimmune disease self-antigens may also be able to modulate the immune system to induce tolerance and therefore either prevent or treat diseases such as T1D and RA.

We engineered the coat proteins of CPMV and TBSV to display immunodominant peptides associated with T1D (p524opt) and RA (pLIP1 or pFADK2), respectively. These viruses are similar in shape and size, but the density of peptide display is threefold lower in CPMV due to the assembly of the virion from two different coat protein subunits, compared to the single coat protein of TBSV. Icosahedral nanoparticles tend to circulate in vivo for a few hours, whereas filamentous and rod-shaped viruses persist for longer, but the residence time in our case should be sufficient to trigger the desired effects (23). We found that the presence of p524opt reduced the yield of CPMV particles in plants by 10-fold compared to the wild-type virus, perhaps due to the loss of stability or promotion of aggregation, although we optimized the pI of the recombinant particles (17). In contrast, the presence of either pLIP1 or pFADK2 improved the yields of TBSV, perhaps by the opposite effect of increasing stability.

We tested the recombinant pVNPs in appropriate mouse models of T1D and RA and compared their efficacy to the corresponding peptides without a virus scaffold. The peptides were administered with an adjuvant, which is necessary to ensure a strong immune response, whereas the pVNPs were administered without an adjuvant, because the repetitive structure of the virus scaffold is known to achieve a similar effect (23). Adjuvants can trigger local or systemic reactogenicity, which negatively affects public perception of the risk-benefit balance of immunization. In contrast, the safety profile of plant viruses is positive, given their ubiquitous presence in the environment and especially in all plant-based foods.

The analysis of NOD mice revealed that two treatments with the CPMV.p524opt formulation achieved partial protection from the onset of diabetes, whereas the free p524opt peptide had no protective effect. The protective mechanism induced by CPMV.p524opt did not appear to be mediated by T_{reg} cells, given that fewer Foxp3$^+$ cells were present around the pancreatic islets of mice treated with the
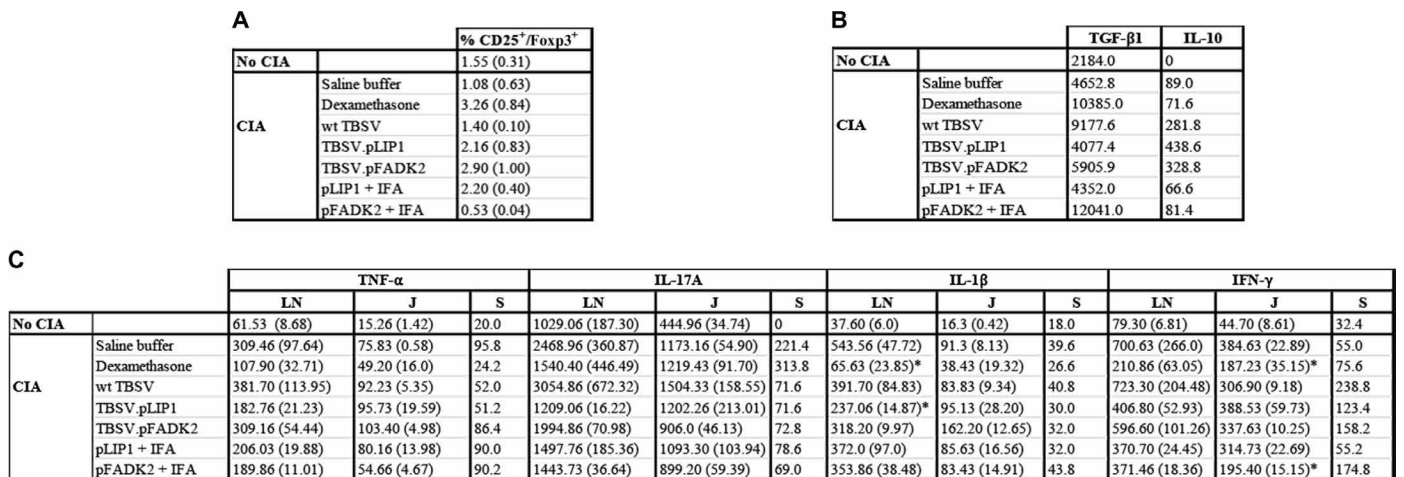
A

		% CD25$^+$/Foxp3$^+$
No CIA		1.55 (0.31)
CIA	Saline buffer	1.08 (0.63)
	Dexamethasone	3.26 (0.84)
	wt TBSV	1.40 (0.10)
	TBSV.pLIP1	2.16 (0.83)
	TBSV.pFADK2	2.90 (1.00)
	pLIP1 + IFA	2.20 (0.40)
	pFADK2 + IFA	0.53 (0.04)

B

		TGF-β1	IL-10
No CIA		2184.0	0
CIA	Saline buffer	4652.8	89.0
	Dexamethasone	10385.0	71.6
	wt TBSV	9177.6	281.8
	TBSV.pLIP1	4077.4	438.6
	TBSV.pFADK2	5905.9	328.8
	pLIP1 + IFA	4352.0	66.6
	pFADK2 + IFA	12041.0	81.4

C

		TNF-α			IL-17A			IL-1β			IFN-γ		
		LN	J	S	LN	J	S	LN	J	S	LN	J	S
No CIA		61.53 (8.68)	15.26 (1.42)	20.0	1029.06 (187.30)	444.96 (34.74)	0	37.60 (6.0)	16.3 (0.42)	18.0	79.30 (6.81)	44.70 (8.61)	32.4
CIA	Saline buffer	309.46 (97.64)	75.83 (0.58)	95.8	2468.96 (360.87)	1173.16 (54.90)	221.4	543.56 (47.72)	91.3 (8.13)	39.6	700.63 (266.0)	384.63 (22.89)	55.0
	Dexamethasone	107.90 (32.71)	49.20 (16.0)	24.2	1540.40 (446.49)	1219.43 (91.70)	313.8	65.63 (23.85)*	38.43 (19.32)	26.6	210.86 (63.05)	187.23 (35.15)*	75.6
	wt TBSV	381.70 (113.95)	92.23 (5.35)	52.0	3054.86 (672.32)	1504.33 (158.55)	71.6	391.70 (84.83)	83.83 (9.34)	40.8	723.30 (204.48)	306.90 (9.18)	238.8
	TBSV.pLIP1	182.76 (21.23)	95.73 (19.59)	51.2	1209.06 (16.22)	1202.26 (213.01)	71.6	237.06 (14.87)*	95.13 (28.20)	30.0	406.80 (52.93)	388.53 (59.73)	123.4
	TBSV.pFADK2	309.16 (54.44)	103.40 (4.98)	86.4	1994.86 (70.98)	906.0 (46.13)	72.8	318.20 (9.97)	162.20 (12.65)	32.0	596.60 (101.26)	337.40 (10.25)	158.2
	pLIP1 + IFA	206.03 (19.88)	80.16 (13.98)	90.0	1497.76 (185.36)	1093.30 (103.94)	78.6	372.0 (97.0)	85.63 (16.56)	32.0	370.70 (24.45)	314.73 (22.69)	55.2
	pFADK2 + IFA	189.86 (11.01)	54.66 (4.67)	90.2	1443.73 (36.64)	899.20 (59.39)	69.0	353.86 (38.48)	83.43 (14.91)	43.8	371.46 (18.36)	195.40 (15.15)*	174.8

Fig. 6. Effect of TBSV-derived particles on cytokine profiles and the proportion of CD25$^+$ Foxp3$^+$ cells. (**A**) The percentage of CD25$^+$ Foxp3$^+$ cells was determined in the lymph nodes of non-CIA mice and CIA mice treated with saline, dexamethasone, wild-type TBSV, TBSV.pLIP1, TBSV.pFADK2, pLIP1 + IFA, and pFADK2 + IFA on day 60 after immunization. Values represent means ± SEM ($n = 3$; except for non-CIA mice, where $n = 2$). (**B**) Levels (pg/ml) of TGFβ1 and IL10 were determined in the serum of non-CIA mice and CIA mice treated with saline, dexamethasone, wild-type TBSV, TBSV.pLIP1, TBSV.pFADK2, pLIP1 + IFA, and pFADK2 + IFA on day 60 after immunization. Serum values represent data pooled from five mice. (**C**) TNFα, IL17A, IL-1β, and IFNγ levels (pg/ml) were determined in the serum (S) and lymph node (LN)/joint (J) supernatants of non-CIA mice and CIA mice treated with saline, dexamethasone, wild-type TBSV, TBSV.pLIP1, TBSV.pFADK2, pLIP1 + IFA, and pFADK2 + IFA on day 60 after immunization. Values represent means ± SEM ($n = 3$). Serum values represent data pooled from five mice. Statistical significance was determined by ANOVA, followed by Bonferroni correction. Values of $P < 0.05$ were considered significant (*). Significance was established for CIA mice treated versus saline-treated + CIA.

pVNP formulation. Similarly, the analysis of recent-onset NOD mice treated with the bacterium *Lactococcus lactis* engineered to secrete GAD65370-575 (and the anti-inflammatory cytokine IL10) in the gut combined with short-course low-dose anti-CD3 (combi-GAD therapy) achieved the stabilization of insulitis, the preservation of functional β-cell mass, and the restoration of normoglycemia, with no significant difference in the number of Foxp3$^+$ cells in and around pancreatic islets compared to untreated mice (6). We speculate that the positive outcomes we observed may reflect the differential activation of cytokines by the various treatment groups, with IL10 and IL2 playing a major role in the double-dose treatment with CPMV.p524.

The analysis of DBA mice following the establishment of CIA provided exciting preliminary evidence that the administration of TBSV particles displaying pFADK2 or pLIP1 can achieve the complete remission of arthritis signs even if the pVNPs are delivered after the onset of disease. CIA in DBA mice is the most commonly used T helper cell (T$_H$1)–dependent model of chronic arthritis, because it is highly reproducible and allows the antibody-induced effector phase of arthritis to be studied in detail. Tolerance to citrullinated proteins has been shown in DBA mice, and the prophylactic administration of citrullinated filaggrin peptide protected these mice from arthritis (24). The administration of a multiepitope citrullinated peptide derived from major prevalent autoantigens immediately after the induction of disease significantly reduced the severity of symptoms in an adjuvant-induced rat arthritis model (25). These results and our data support the hypothesis that antigen-specific tolerance can be achieved in RA by the repeated administration of peptides that cause the immunomodulation of T cell populations involved in the immune response (mainly T$_H$1, T$_H$17, and T$_{reg}$ cells) and the down-regulation of proinflammatory cytokines. Specifically, we observed the depletion of TNFα, IL1β, IL17, and IFNγ in the serum, lymph nodes, and (to a lesser extent) the joints. These cytokines are the key mediators of the innate (TNFα), adaptive (IFNγ), and T$_H$17-mediated

(IL17) immune responses in RA. The beneficial effect of the pVNPs was also associated with the secretion of anti-inflammatory cytokines such as IL10 for TBSV.pLIP1 and TBSV.pFADK2, and both TGFβ and IL10 for TBSV.pFADK2, as well as the accumulation of CD25$^+$ Foxp3$^+$ T$_{reg}$ cells, which suppress autoreactive lymphocytes either by direct contact or by promoting the secretion of TGFβ and IL10. The higher proportion of T$_{reg}$ cells in the lymph nodes of treated mice supports the role of this T cell subset in suppressing the immune-mediated inflammation that occurs during the pathogenesis of RA (25).

The roles of liprins and FADKs (focal adhesion kinases) in the immunopathogenesis of RA are unknown. The liprin family of multidomain proteins is required for cell motility on the extracellular matrix and the efficient regulation of focal adhesion during cell migration (26). The liprin α1 dimer is strongly expressed by lymphatic endothelial cells, where it regulates lymphatic vessel integrity (27). The pFADK2 sequence was derived from protein tyrosine kinase 2β (FAK2/PTK2B), which controls cell adhesion, migration, and invasion. In murine models of RA, FAK2/PTK2B promotes inflammatory angiogenesis, induces synovial fibroblast invasion, and triggers the formation of synovial pannus, suggesting a role in the onset and progression of synovial hyperplasia (28, 29). The positive effect of pFADK2 administration in DBA mice may therefore partially reflect the inhibition of synovial hyperplasia, supporting the role of focal adhesion kinases in the pathogenesis of RA and the value of peptide-driven therapy using adjuvant viral scaffolds.

Together, our results indicate that although immunodominant peptides delivered by pVNPs offer a therapeutic benefit in models of both T1D and RA, the underlying mechanisms are different, with the activation of T$_{reg}$ cells required only in the RA model. This shows that the peptides displayed by the pVNP strongly influence the immunomodulatory mode of action. However, the virus scaffold achieved an adjuvant effect in both cases, perhaps by stabilizing the peptide and concentrating multiple peptides in a small area. The

combination of virus scaffold and immunodominant peptides resulted in the secretion of IL10, which was more abundant in the serum of both disease models after treatment with the pVNP. The requirement for both the scaffold and the peptides is shown by the negligible increase in IL10 levels in response to either the wild-type virus or the synthetic peptide formulation.

MATERIALS AND METHODS
Gene cloning and transient expression
The sequence encoding the p524opt peptide (DSRLSKVAP-VIKARMMED) (30) was codon-optimized for *N. benthamiana* and transferred to vector pEAQ-HT-VP60 as previously described (31) to generate the recombinant plasmid pEAQ-HT-VP60.p524opt. The sequences encoding the peptides pLIP1 (ASVLANVAQAFE) and pFADK2 (AKVLANLAHPPA) (16) were likewise codon-optimized and transferred to the TBSV expression plasmid as previously described (18).

The transient expression of CPMV vectors was achieved by introducing pEAQ-HT-VP60.p524opt (or pEAQ-HT-VP60 as a control) along with pEAQ-HT-24K into *A. tumefaciens* strain LBA4404 (32). We manually infiltrated four leaves in 3 or 30 *N. benthamiana* plants depending on the scale of expression and isolated the pVNPs 6 dpi. The transient expression of TBSV vectors was achieved by in vitro transcription to produce infectious RNAs, which were used for the manual infection of two leaves in three *N. benthamiana* plants. Leaves displaying local and systemic infection symptoms were pooled and checked for recombinant virus RNA by reverse transcription polymerase chain reaction (RT-PCR). Sap was collected from the infected leaves 6 to 10 dpi (depending on the construct) and used for the secondary large-scale infection of 50 plants. The pVNPs were isolated 6 to 10 days later, following the appearance of infection symptoms.

Purification of pVNPs
The pVNPs were purified as previously described (33, 34). For CPMV, 25 to 30 g of infiltrated leaf tissue were extracted (34), and the green juice was processed by anion-exchange chromatography (DEAE Sephadex A-50 resin) to remove impurities. The flow-through fraction was collected and concentrated 30-fold using 100-kDa cutoff Centricon tubes. The pVNPs were then isolated from the concentrate by size exclusion chromatography using a HiPrep 16/60 Sephacryl S-500 HR (ÄKTAprime plus) column. For TBSV, we collected 30 to 40 g of mixed symptomatic and locally infected leaves, and the green juice was extracted as previously described (18). Briefly, after filtration, the extract was incubated in ice for 1 hour and centrifuged at 8000*g* for 15 min at 4°C. The supernatant was collected and centrifuged at 90,000*g* for 1 hour at 4°C. The pellet was then resuspended in 50 mM sodium acetate (pH 5.3), and the resulting solution was centrifuged at 8000*g* for 15 min at 4°C. The supernatant was collected and stored at −20°C.

Western blot, DLS, and TEM analysis
To confirm the presence, integrity, and structure of the pVNPs, total soluble protein was extracted from infiltrated leaves and analyzed by SDS–polyacrylamide gel electrophoresis and silver staining, Western blot (CPMV only), DLS, and TEM as previously described (33). CPMV particles were detected using primary polyclonal antibody G49 diluted to 1:2000 as previously described (33).

Ethics statement
All procedures involving animals conformed to national and international laws and policies. All animal experiments met the requirements of European Union Directive 2010/63, the European Convention for Protection of Vertebrate Animals used for Experimental and other Scientific Purposes, and National Law 116/92. The protocol was approved by the Animal Care and Use Committee of the University of Perugia and by the Italian Ministry of Health. All animals were housed in the animal facility of the University of Perugia (authorization number 34/2003A).

Animal studies involving NOD mice
Four-week-old female NOD mice were obtained from Charles River Laboratories and housed under specific pathogen–free conditions in the animal facility at the University of Perugia, with ad libitum access to water and food. NOD mice were randomly subdivided into four groups. In group 1 (*n* = 18), CPMV.p524opt [50 μg per mouse, resuspended in 100 μl of phosphate-buffered saline (PBS)] was injected twice intraperitoneally, with 2 weeks between doses. In group 2 (*n* = 20), wild-type CPMV particles (50 μg per mouse, resuspended in 100 μl of PBS) were administered with the same schedule. In group 3 (*n* = 15), synthetic peptide p524 (50 μg per mouse, resuspended in 100 μl of PBS plus IFA) was administered with the same schedule. In group 4 (*n* = 15), the same schedule and dosing was used for synthetic peptide p524opt. Another group of NOD mice (*n* = 14) received a single dose of CPMV.p524 (50 μg per mouse, resuspended in 100 μl of PBS). A control group was left untreated (*n* = 20). Mice were monitored for the appearance of clinical signs of diabetes and were euthanized when the disease was confirmed by glucosuria.

Animal studies involving DBA mice
Female DBA/1 mice 6 to 8 weeks of age (Charles River Laboratories) were maintained under specific pathogen–free conditions as above. CIA was induced by the intradermal tail base injection of 100 μg of chicken type II collagen (Sigma-Aldrich) as previously described (35). Five mice per group were immunized on days 0 and 21 to induce arthritis. The onset of disease was confirmed on the day that swelling or erythema was observed in any paw, typically 4 to 10 days after the second immunization. Each experimental group was treated seven times, 5 days apart, starting from day 28 after the first immunization, with intraperitoneal injections of saline (200 μl per mouse), TBSV.pLIP1, TBSV.pFADK2, pLIP1 + IFA, and pFADK2 + IFA (all 50 μg per mouse in 200 μl) or dexamethasone (5 μg per mouse in 200 μl). A healthy nonimmunized group (*n* = 5) was included as a control. CIA was assessed using a macroscopic score system based on the visual identification of arthritic limbs. The clinical severity of arthritis was evaluated as follows: Each mouse was inspected every 2 to 3 days for three different parameters: (i) swelling of the hind ankle and foot, measured with calipers; (ii) erythema of each leg; and (iii) swelling of the fingers. Each of these parameters was assessed by severity and was graded from 0 to 4 as shown in fig. S2. The RA index for each mouse was expressed as the mean of the three scores from the individual parameters. At the end of the experiment (60 days), we determined the proportion of CD25$^+$ Foxp3$^+$ cells in the lymph nodes and measured cytokine titers in the lymph nodes, joints, and serum (see below).

Histopathological analysis of treated mice
For histology and immunohistochemistry, mice were euthanized 5, 10, and 27 weeks after treatment. The pancreas was removed and fixed

in 10% buffered formalin for 20 hours and embedded in paraffin. Sections of 5 mm were cut 40 μm apart throughout the gland and stained with hematoxylin-eosin (Merck) to determine the insulitis score using the following grading scale: 0, intact islet; 1, peri-insulitis; 2, moderate insulitis (<50% of the islet infiltrated); and 3, severe insulitis (≥50% of the islet infiltrated). At least 15 islets per pancreas were analyzed by two independent examiners as previously described (6). Some sections, after deparaffinization and rehydration through an ethanol series, were analyzed by double immunofluorescence staining for Foxp3 and insulin (36). The number of Foxp3$^+$ cells within and around pancreatic islets was determined by manual counting.

Cytokine determination
In the serum of NOD mice, 23 cytokines [IL1α, IL1β, IL2, IL3, IL4, IL5, IL6, IL9, IL10, IL12 (p40), IL12 (p70), IL13, IL17A, eotaxin, G-CSF (granulocyte colony-stimulating factor), GM-CSF (granulocyte-macrophage CSF), IFNγ, KC, MCP1 (MCAF), MIP1α, MIP1β, RANTES, and TNFα] were quantified using Luminex xMAP technology (Bio-Plex Pro Mouse Cytokine 23-Plex, Bio-Rad Laboratories). To quantify cytokines in DBA mice, joint tissues were pulverized and resuspended in 1 ml of lysis medium per 100-mg joint weight for 60 min at 37°C, followed by centrifugation to remove debris. Lymph nodes were removed, homogenized, and centrifuged as above. Supernatants from both preparations were sterilized by passing through a Millipore filter (0.45 μm pore size) and stored at −80°C. TNFα, IL17A, IL1β, IFNγ, TGFβ1, and IL10 concentrations were determined in serum and supernatants using commercial enzyme-linked immunosorbent assay kits (eBioscience) according to the manufacturer's recommendations.

Statistical analysis
For studies in NOD mice, diabetes-free survival in the treatment groups was compared by Kaplan-Meier analysis with a log-rank test. The Mann-Whitney U test was used to compare insulitis scores among different groups.

OPLS-DA was used to integrate principal components analysis data and reduce experimental variability and was performed using SIMCA PLUS v13.0 (Umetrics). To define the number of classes for the OPLS-DA model, we applied partial cross-validation and a permutation test to reveal overfitting.

For DBA/1 mice, quantitative variables were tested for normal distribution in GraphPad Prism v7. Statistical differences in cytokine levels between treatment groups were determined by analysis of variance (ANOVA), followed by Bonferroni's test. Statistical differences in the arthritic score and number of T_{reg} cells detected in the lymph nodes of RA mice were determined by applying the Kruskal-Wallis test followed by Dunn's multiple comparison test. A value of $P < 0.05$ was considered significant.

SUPPLEMENTARY MATERIALS
Supplementary material for this article is available at http://advances.sciencemag.org/cgi/content/full/6/19/eaaz0295/DC1

View/request a protocol for this paper from *Bio-protocol*.

REFERENCES AND NOTES
1. A. M. Wen, N. F. Steinmetz, Design of virus-based nanomaterials for medicine, biotechnology, and energy. *Chem. Soc. Rev.* **45**, 4074–4126 (2016).
2. K. J. Koudelka, A. S. Pitek, M. Manchester, N. F. Steinmetz, Virus-based nanoparticles as versatile nanomachines. *Annu Rev Virol.* **2**, 379–401 (2015).
3. J. Röder, C. Dickmeis, U. Commandeur, Small, smaller, nano: New applications for Potato virus X in nanotechnology. *Front. Plant Sci.* **10**, 158 (2019).
4. L. K. Lee, R. M. Twyman, S. Fiering, N. F. Steinmetz, Virus-based nanoparticles as platform technologies for modern vaccines. *Wiley Interdiscip. Rev. Nanomed. Nanobiotechnol.* **8**, 554–578 (2016).
5. J. L. Chiang, M. S. Kirkman, L. M. Laffel, A. L. Peters, Type 1 Diabetes Sourcebook, Type 1 diabetes through the life span: A position statement of the American Diabetes Association. *Diabetes Care* **37**, 2034–2054 (2014).
6. S. Robert, C. Gysemans, T. Takiishi, H. Korf, I. Spagnuolo, G. Sebastiani, K. Van Huynegem, L. Steidler, S. Caluwaerts, P. Demetter, C. H. Wasserfall, M. A. Atkinson, F. Dotta, P. Rottiers, T. L. Van Belle, C. Mathieu, Oral delivery of glutamic acid decarboxylase (GAD)-65 and IL10 by *Lactococcus lactis* reverses diabetes in recent-onset NOD mice. *Diabetes* **63**, 2876–2887 (2014).
7. T. L. Delovitch, B. Singh, The nonobese diabetic mouse as a model of autoimmune diabetes: Immune dysregulation gets the NOD. *Immunity* **7**, 727–738 (1997).
8. R. Tisch, B. Wang, D. V. Serreze, Induction of glutamic acid decarboxylase 65-specific Th2 cells and suppression of autoimmune diabetes at late stages of disease is epitope dependent. *J. Immunol.* **163**, 1178–1187 (1999).
9. T. Ogino, K. Sato, N. Miyokava, S. Kimura, M. Katagiri, Importance of GAD65 peptides and I-A^{97} in the development of insulitis in nonobese diabetic mice. *Immunogenetics* **51**, 538–545 (2000).
10. G. Chen, G. Han, J. Feng, J. Wang, R. Wang, R. Xu, B. Shen, J. Qian, Y. Li, Glutamic acid decarboxylase-derived epitopes with specific domains expand CD4$^+$CD25$^+$ regulatory T cells. *PLOS ONE* **4**, e7034 (2009).
11. P. Saï, A. S. Rivereau, C. Granier, T. Haertlé, L. Martignat, Immunization of non-obese diabetic (NOD) mice with glutamic acid decarboxylase-derived peptide 524–543 reduces cyclophosphamide-accelerated diabetes. *Clin. Exp. Immunol.* **105**, 330–337 (1996).
12. J. Tian, M. A. Atkinson, M. Clare-Salzler, A. Herschenfeld, T. Forsthuber, P. V. Lehmann, D. L. Kaufman, Nasal administration of glutamate decarboxylase (GAD65) peptides induces Th2 responses and prevents murine insulin-dependent diabetes. *J. Exp. Med.* **183**, 1561–1567 (1996).
13. V. Majithia, S. A. Geraci, Rheumatoid arthritis: Diagnosis and management. *Am. J. Med.* **120**, 936–939 (2007).
14. L. B. Nordberg, S. Lillegraven, A.-B. Aga, J. Sexton, I. C. Olsen, E. Lie, H. Berner Hammer, T. Uhlig, D. van der Heijde, T. K. Kvien, E. A. Haavardsholm, Comparing the disease course of patients with seronegative and seropositive rheumatoid arthritis fulfilling the 2010 ACR/EULAR classification criteria in a treat-to-target setting: 2-year data from the ARCTIC trial. *RMD Open* **4**, e000752 (2018).
15. K. Somers, P. Geusens, D. Elewaut, F. De Keyser, J.-L. Rummens, M. Coenen, M. Blom, P. Stinissen, V. Somers, Novel autoantibody markers for early and seronegative rheumatoid arthritis. *J Autoimm.* **36**, 33–46 (2011).
16. E. Bartoloni Bocci, E. Pericolini, E. Tinazzi, E. Gabrielli, A. Falorni, M. Pezzotti, R. Gerli, C. Lunardi, A. Vecchiarelli, L. Avesani, Immunomodulazione di un modello di artrite reumatoide con peptidi prodotti in piattaforme vegetali. 56° Congresso Nazionale Società Italiana Reumatologia. *Reumatismo* **71**, 91–92 (2019).
17. C. Porta, V. E. Spall, K. C. Findlay, R. C. Gergerich, C. E. Farrance, G. P. Lomonossoff, Cowpea mosaic virus-based chimaeras: Effects of inserted peptides on the phenotype, host range, and transmissibility of the modified viruses. *Virology* **310**, 50–63 (2003).
18. S. Grasso, C. Lico, F. Imperatori, L. Santi, Plant derived multifunctional tool for nanobiotechnology based on *Tomato bushy stunt virus*. *Transgenic Res.* **22**, 519–535 (2013).
19. E. Schurgers, A. Billiau, P. Matthys, Collagen-induced arthritis as an animal model for rheumatoid arthritis: Focus on interferon-γ. *J. Interferon Cytokine Res.* **31**, 917–926 (2011).
20. G. T. Jennings, M. F. Bachmann, Immunodrugs: Therapeutic VLP-based vaccines for chronic diseases. *Annu. Rev. Pharmacol. Toxicol.* **49**, 303–326 (2009).
21. M. R. Sheen, P. H. Lizotte, S. Toraya-Brown, S. Fiering, Stimulating antitumor immunity with nanoparticles. *Wiley Interdiscip. Rev. Nanomed. Nanobiotechnol.* **6**, 496–505 (2014).
22. P. H. Lizotte, A. M. Wen, M. R. Sheen, J. Fields, P. Rojanasopondist, N. F. Steinmetz, S. Fiering, *In situ* vaccination with cowpea mosaic virus nanoparticles suppresses metastatic cancer. *Nat. Nanotechnol.* **11**, 295–303 (2016).
23. Y. Geng, P. Dalhaimer, S. Cai, R. Tsai, M. Tewari, T. Minko, D. E. Discher, Plant-produced potato virus X chimeric particles displaying an influenza virus-derived peptide activate specific CD8+ T cells in mice. *Nat. Nanotechnol.* **2**, 249–255 (2007).
24. S. Gertel, G. Serre, Y. Shoenfeld, H. Amital, Immune tolerance induction with multiepitope peptide derived from citrullinated autoantigens attenuates arthritis manifestations in adjuvant arthritis rats. *J. Immunol.* **194**, 5674–5680 (2015).
25. N. Komatsu, H. Takayanagi, Arthritogenic T cells in autoimmune arthritis. *Intern. J. Biochem. Cell Biol.* **58**, 92–96 (2015).
26. V. Astro, S. Chiaretti, E. Magistrati, M. Fivaz, I. de Curtis, Liprin-α1, ERC1 and LL5 define polarized and dynamic structures that are implicated in cell migration. *J. Cell Sci.* **127**, 3862–3876 (2014).
27. C. Norrmén, W. Vandevelde, A. Ny, P. Saharinen, M. Gentile, G. Haraldsen, P. Puolakkainen, E. Lukanidin, M. Dewerchin, K. Alitalo, T. V. Petrova, Liprin β1 is highly expressed

in lymphatic vasculature and is important for lymphatic vessel integrity. *Blood* **115**, 906–909 (2010).

28. H.-Y. Gao, J. Luo, X.-F. Li, Q. Lv, H.-Y. Wen, Q.-Z. Song, W.-P. Zhao, X.-C. Zhao, T.-T. Zhang, S.-Y. Zhang, J.-M. Zhi, Changes in focal adhesion kinase expression in rats with collagen-induced arthritis and efficacy of intervention with disease modifying anti-rheumatic drugs alone or in combination. *Int. J. Clin. Exp. Pathol.* **8**, 15573–15581 (2015).

29. M. A. Shelef, D. A. Bennin, N. Yasmin, T. F. Warner, T. Ludwig, H. E. Beggs, A. Huttenlocher, Focal adhesion kinase is required for synovial fibroblast invasion, but not murine inflammatory arthritis. *Arthritis Res. Ther.* **16**, 464 (2014).

30. Y. D. Dai, K. P. Jensen, A. Lehuen, E. L. Masteller, J. A. Bluestone, D. B. Wilson, E. E. Sercarz, A peptide of glutamic acid decarboxylase 65 can recruit and expand a diabetogenic T cell clone, BDC2.5, in the pancreas. *J. Immunol.* **175**, 3621–3627 (2005).

31. F. Sainsbury, P. Saxena, A. A. A. Aljabali, K. Saunders, D. J. Evans, G. P. Lomonossoff, Genetic engineering and characterization of cowpea mosaic virus empty virus-like particles. *Methods Mol. Biol.* **1108**, 139–153 (2014).

32. E. Tinazzi, M. Merlin, C. Bason, R. Beri, R. Zampieri, C. Lico, E. Bartolini, A. Puccetti, C. Lunardi, M. Pezzotti, L. Avesani, Plant-derived chimeric virus particles for the diagnosis of primary Sjögren syndrome. *Front. Plant Sci.* **6**, 1080 (2015).

33. K. Saunders, F. Sainsbury, G. P. Lomonossoff, Efficient generation of *cowpea mosaicvirus* empty virus-like particles by the proteolytic processing of precursors in insect cells and plants. *Virology* **393**, 329–337 (2009).

34. D. D. Brand, K. A. Latham, E. F. Rosloniec, Collagen-induced arthritis. *Nat. Protoc.* **2**, 1269–1275 (2007).

35. T. Takiishi, H. Korf, T. L. Van Belle, S. Robert, F. A. Grieco, S. Caluwaerts, L. Galleri, I. Spagnuolo, L. Steidler, K. Van Huynegem, P. Demetter, C. Wasserfall, M. A. Atkinson, F. Dotta, P. Rottiers, C. Gysemans, C. Mathieu, Reversal of autoimmune diabetes by restoration of antigen-specific tolerance using genetically modified *Lactococcus lactis* in mice. *J. Clin. Invest.* **122**, 1717–1725 (2012).

36. D. van der Woude, A. H. M. van der Helm-van Mil, Update on the epidemiology, risk factors, and disease outcomes of rheumatoid arthritis. *Best Pract. Res. Clin. Rheumatol.* **32**, 174–187 (2018).

Citation: R. Zampieri, A. Brozzetti, E. Pericolini, E. Bartoloni, E. Gabrielli, E. Roselletti, G. Lomonosoff, Y. Meshcheriakova, L. Santi, F. Imperatori, M. Merlin, E. Tinazzi, F. Dotta, L. Nigi, G. Sebastiani, M. Pezzotti, A. Falorni, L. Avesani, Prevention and treatment of autoimmune diseases with plant virus nanoparticles. *Sci. Adv.* **6**, eaaz0295 (2020).

Science Advances

Prevention and treatment of autoimmune diseases with plant virus nanoparticles

Roberta Zampieri, Annalisa Brozzetti, Eva Pericolini, Elena Bartoloni, Elena Gabrielli, Elena Roselletti, George Lomonosoff, Yulia Meshcheriakova, Luca Santi, Francesca Imperatori, Matilde Merlin, Elisa Tinazzi, Francesco Dotta, Laura Nigi, Guido Sebastiani, Mario Pezzotti, Alberto Falorni and Linda Avesani

ARTICLE TOOLS	http://advances.sciencemag.org/content/6/19/eaaz0295
SUPPLEMENTARY MATERIALS	http://advances.sciencemag.org/content/suppl/2020/05/04/6.19.eaaz0295.DC1
REFERENCES	This article cites 36 articles, 9 of which you can access for free http://advances.sciencemag.org/content/6/19/eaaz0295#BIBL
PERMISSIONS	http://www.sciencemag.org/help/reprints-and-permissions

Use of this article is subject to the Terms of Service